JACS
JOURNAL OF THE AMERICAN CHEMICAL SOCIETY

Article

pubs.acs.org/JACS

# Dramatically Different Kinetics and Mechanism at Solid/Liquid and Solid/Gas Interfaces for Catalytic Isopropanol Oxidation over Size-Controlled Platinum Nanoparticles

Hailiang Wang,[†,‡,§] Andras Sapi,[†,‡,§] Christopher M. Thompson,[†,‡,§] Fudong Liu,[†,‡] Danylo Zherebetskyy,[‡] James M. Krier,[†,‡] Lindsay M. Carl,[†,‡] Xiaojun Cai,[†,‡] Lin-Wang Wang,[‡] and Gabor A. Somorjai*[,†,‡]

[†]Department of Chemistry, University of California, Berkeley, California 94720, United States

[‡]Materials Sciences Division, Lawrence Berkeley National Laboratory, Berkeley, California 94720, United States

Supporting Information

**ABSTRACT:** We synthesize platinum nanoparticles with controlled average sizes of 2, 4, 6, and 8 nm and use them as model catalysts to study isopropanol oxidation to acetone in both the liquid and gas phases at 60 °C. The reaction at the solid/liquid interface is 2 orders of magnitude slower than that at the solid/gas interface, while catalytic activity increases with the size of platinum nanoparticles for both the liquid-phase and gas-phase reactions. The activation energy of the gas-phase reaction decreases with the platinum nanoparticle size and is in general much higher than that of the liquid-phase reaction which is largely insensitive to the size of catalyst nanoparticles. Water substantially promotes isopropanol oxidation in the liquid phase. However, it inhibits the reaction in the gas phase. The kinetic results suggest different mechanisms between the liquid-phase and gas-phase reactions, correlating well with different orientations of IPA species at the solid/liquid interface vs the solid/gas interface as probed by sum frequency generation vibrational spectroscopy under reaction conditions and simulated by computational calculations.

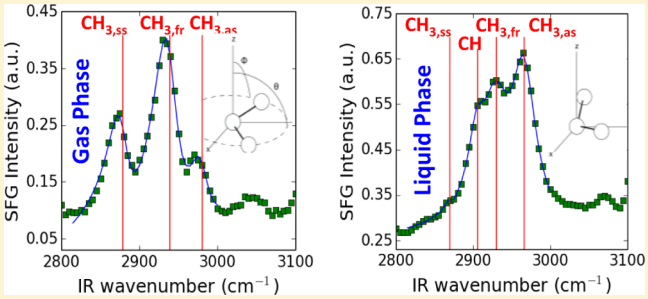


## INTRODUCTION

Oxidation of alcohols is useful for chemical production and energy conversion. While full oxidation of alcohols to carbon dioxide is desirable for direct alcohol fuel cells,[1,2] partial oxidation to aldehydes, ketones, and carboxylic acids is needed to produce various compounds.[3,4] Oxidizing alcohols with molecular oxygen using heterogeneous catalysts in the liquid phase especially in aqueous solutions is a method of high efficiency and low environmental impact for synthesizing fine chemicals.

Platinum and its alloys are important catalysts for many chemical reactions including alcohol oxidation.[5−7] Chemo-, regio-, and stereoselective oxidations of carbohydrates are particularly valuable processes.[3] For structure sensitive reactions, the catalytic performance of platinum nanoparticles can be highly dependent on their sizes.[8−12] For example, in a furfural decarbonylation/hydrogenation reaction carried out in the gas phase, platinum nanoparticles with various sizes in the range 1.5−7.1 nm exhibit significantly different product selectivities, turnover rates, and apparent activation energies.[11] Such size dependence would have been easily rendered undetectable if polydispersed nanoparticle catalysts made by conventional impregnation methods had been used. It is therefore critical to employ colloidal synthesis to tune the size of platinum nanoparticles while keeping other structural parameters the same in order to investigate structure sensitivity of platinum nanoparticles in catalysis.[13] Since most of such studies have been carried out for gas phase reactions,[8−12] it becomes highly important to compare the size-dependent catalytic behavior of platinum nanoparticles in gas-phase vs liquid-phase reactions.

There are organic molecules whose catalytic reaction kinetics and mechanisms can be studied at both the solid/liquid and solid/gas interfaces. Oxidations of many alcohols belong to these classes of reactions. However, these are rarely studied at both interfaces to determine how changes in reaction conditions from gas to liquid alter the reaction mechanisms, although the large differences in density of reactants would likely alter the reaction kinetics. In this paper we investigate the platinum catalyzed oxidation of isopropyl alcohol (IPA) to acetone at both solid/liquid and solid/gas interfaces and find dramatically different kinetics and mechanisms. We find that in the gas phase platinum nanoparticles have 2 orders of magnitude faster IPA oxidation turnover rates than in the liquid phase. Like most metal catalyzed reactions that are carried out on monodispersed nanoparticles, the size of the nanoparticles changes the reaction rates and often the reaction

**Received:** June 5, 2014
**Published:** July 3, 2014

   dx.doi.org/10.1021/ja505641r | J. Am. Chem. Soc. 2014, 136, 10515−10520

selectivities (structure sensitivity). In IPA oxidation, the turnover rates increase by a factor of ∼7 with increasing catalyst particle sizes in the 2−8 nm range in both the gas and liquid phases. The activation energies of IPA oxidation on platinum nanoparticles are much higher in the gas phase (∼170 kJ/mol) as compared to the liquid phase (∼60 kJ/mol). The addition of liquid water as a diluent to liquid IPA accelerates catalytic oxidation while water vapor inhibits the oxidation in the gas phase. The kinetic results suggest different mechanisms between the liquid-phase and gas-phase reactions, correlating well with different orientations of IPA species at the solid/liquid and solid/gas interfaces as probed by sum frequency generation (SFG) vibrational spectroscopy under reaction conditions and also simulated by computational calculations.

## RESULTS

Pt nanoparticles with various sizes were synthesized with colloidal methods where polyvinylpyrrolidone (PVP) was used as the capping agent and polyol as the solvent and reducing agent (see Supporting Information (SI) for details). Transmission electron microscopy (TEM) images of the synthesized Pt nanoparticles are shown in Figure 1. The PVP-capped

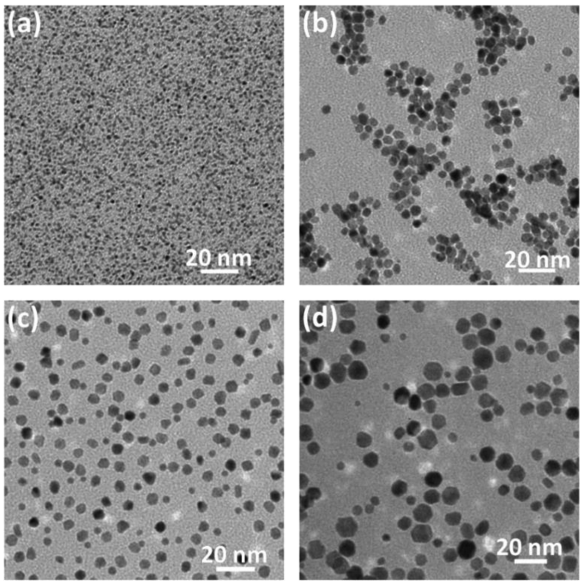


**Figure 1.** Size controlled Pt nanoparticles. (a−d) TEM images of synthesized Pt nanoparticles with average sizes of 2, 4, 6, and 8 nm.

nanoparticles exhibited nearly spherical shapes (Figure 1) and narrow size distributions (Figure S1), affording material systems suitable for the study of size effects in catalyzing liquid-phase and gas-phase IPA oxidation reactions.

IPA oxidation reactions were carried out in both the liquid and gas phases using Pt nanoparticles loaded on mesoporous silica (Figure S2) as catalysts (see SI for details). Liquid-phase catalysis was performed in sealed vials with magnetic stirring. Gas-phase catalysis was carried out in a batch-mode reactor equipped with a boron nitride substrate heater and a metal bellows circulation pump for gas mixing. The reactant and product were detected by gas chromatography (GC) with a flame ionization detector. For all the Pt nanoparticle catalysts tested, acetone was the only product of the reaction.

**A. Gas-Phase IPA Oxidation Catalyzed by Pt Nanoparticles Is 2 Orders of Magnitude Faster than in the Liquid Phase.** For reactions in pure liquid IPA at 60 °C (where the concentrations of IPA and $O_2$ were about 13.3 M and 1.6 mM respectively), turnover frequency (TOF) values between 0.046 and 0.302 molecules·site$^{-1}$·s$^{-1}$ were observed for Pt nanoparticles with various sizes (Figure 2 red data points).

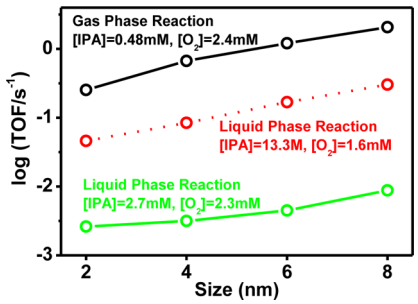


**Figure 2.** Comparison of turnover rates in the gas-phase and liquid-phase IPA oxidation reactions catalyzed by Pt nanoparticles with various sizes. Under the gas-phase reaction condition (black data points), the IPA concentration was much lower than that in pure liquid-phase IPA (red data points). To correct that effect and compare the reaction rates under comparable reactant concentration conditions, we diluted liquid IPA with heptane (green data points) to a concentration comparable to that in the gas phase.

For gas-phase reactions at 60 °C, TOF values between 0.25 and 2.07 molecules·site$^{-1}$·s$^{-1}$ were observed for Pt nanoparticles with various sizes (Figure 2 black data points). In the gas-phase reaction, the IPA concentration was ∼0.48 mM, ∼4 orders of magnitude lower than that in the liquid-phase reaction (pure IPA), and the oxygen concentration was ∼2.4 mM, comparable to that in the liquid phase. But the TOF values of the gas-phase reactions were about ∼5−10 times higher than those of the liquid-phase reactions (black vs red data points).

To assess the reaction rates of IPA oxidation in both the liquid and gas phases under comparable reactant concentration conditions, we diluted IPA with heptane in the liquid phase. We found heptane to be a neutral solvent for IPA oxidation reactions in the liquid phase, as evidenced by the similar conversion rate, size dependence, and activation energy to those in pure liquid IPA (Figure S3). As a saturated hydrocarbon, we believe heptane does not adsorb strongly on the Pt surface. Therefore, the active Pt sites are not blocked by heptane and the reaction mechanism of IPA oxidation is not altered. Moreover, the solubility of oxygen in heptane is close to that in IPA.[14,15] When the IPA concentration in the liquid phase was reduced by dilution with heptane to the same magnitude as that in the gas phase, the reactions in the liquid phase were about 100 times slower than the gas-phase reactions (Figure 2, black vs green data points). The results therefore suggest a 2 orders of magnitude slower kinetics at the solid/liquid interface than the solid/gas interface.

**B. Both the Gas-Phase and Liquid-Phase IPA Oxidation Turnover Rates Are Structure Sensitive: Increasing with Pt Nanoparticles Size by a Factor of 7 from 2 to 8 nm.** For both the liquid-phase and gas-phase reactions, the activity of the catalyst was highly dependent on the size of Pt nanoparticles. In pure liquid IPA at 60 °C, a TOF of ∼0.046 molecules·site$^{-1}$·s$^{-1}$ was observed for 2 nm Pt nanoparticles (Figure 3), which increased to ∼0.084 molecules·site$^{-1}$·s$^{-1}$ when 4 nm nanoparticles were used as the catalyst (Figure 3). The 6 and 8 nm nanoparticles showed even higher catalytic activities, with the corresponding TOF values being


dx.doi.org/10.1021/ja505641r | J. Am. Chem. Soc. 2014, 136, 10515−10520

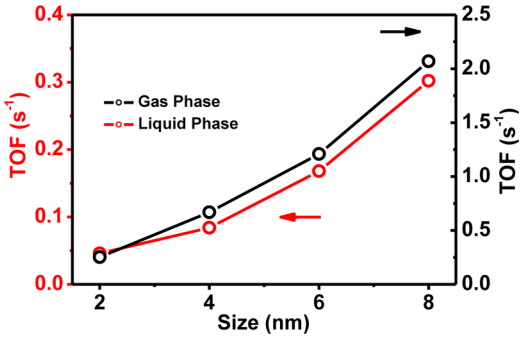


**Figure 3.** Comparison of size dependence of turnover rates in the gas-phase and liquid-phase IPA oxidation reactions catalyzed by Pt nanoparticles with various sizes.

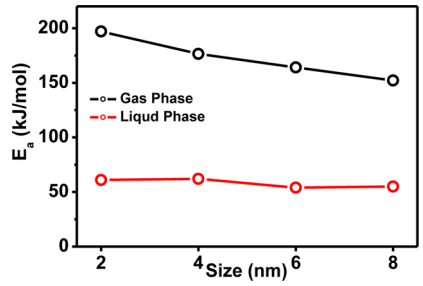


**Figure 4.** Comparison of activation energies in the gas-phase and liquid-phase IPA oxidation reactions catalyzed by Pt nanoparticles with various sizes.

0.168 and 0.302 molecules·site$^{-1}$·s$^{-1}$, respectively (Figure 3), corresponding to an ∼7 times increase in turnover rates in the size range of 2−8 nm. In the gas phase at 60 °C, a similar size dependence of catalytic activity was observed as in the liquid phase. The TOF increased with the size of Pt nanoparticles in the range of 2−8 nm (Figure 3). The 2 nm Pt nanoparticles showed a TOF of ∼0.25 molecules·site$^{-1}$·s$^{-1}$, which increased to ∼0.67 molecules·site$^{-1}$·s$^{-1}$ for 4 nm nanoparticles, ∼1.21 molecules·site$^{-1}$·s$^{-1}$ for 6 nm nanoparticles, and ∼2.07 molecules·site$^{-1}$·s$^{-1}$ for 8 nm nanoparticles, corresponding to an ∼8 times increase in turnover rates in the size range.

A similar trend of increasing specific activity with increasing particle sizes has also been observed for Pt nanoparticles in electrocatalytic methanol oxidation and oxygen reduction reactions.[16−19] Pt nanoparticles with smaller sizes have larger fractions of corner and edge atoms on their surface that can bind certain oxygenated species more strongly than face atoms.[16−19] The adsorption strength of the oxygenated species could pose significant influences on catalytic activity. It has been suggested that dehydrogenation of IPA on the catalyst surface is the rate-determining step.[20,21] Stronger binding of oxygenated species on the catalyst surface may block active sites for IPA adsorption and consequently reduce the TOF for smaller Pt nanoparticles.

**C. Activation Energies of IPA Oxidation on Pt Nanoparticles Are Much Higher in the Gas Phase (∼170 kJ/mol) than in the Liquid Phase (∼60 kJ/mol).** The temperature dependence of IPA oxidation reactions catalyzed by Pt nanoparticles with different sizes was studied in both the liquid and gas phases (Figure S4, S5). Reactions in pure liquid IPA exhibited an activation energy of between 54 and 62 kJ/mol, insensitive to the size of Pt nanoparticle catalysts (Figure 4). In the gas phase, the reaction exhibited a significantly higher activation energy with a stronger dependence on the size of the Pt nanoparticles than the liquid-phase reaction. The 2 nm Pt nanoparticles showed an activation energy of 197 kJ/mol, which decreased monotonically to 176 kJ/mol for 4 nm nanoparticles, 164 kJ/mol for 6 nm nanoparticles, and 152 kJ/mol for 8 nm nanoparticles (Figure 4). Such differences in magnitude and size dependence of activation energy in the liquid-phase reaction as compared to the gas-phase reaction indicate different reaction mechanisms at the solid/liquid interface as compared to the solid/gas interface.

**D. Liquid Water Accelerates the IPA Oxidation Catalyzed by Pt Nanoparticles While Water Vapor Inhibits the Reaction in the Gas Phase.** We took 4 nm Pt nanoparticles as model catalysts to investigate the effect of water on IPA oxidation in both the liquid and gas phases. When IPA was diluted with water in a volume ratio of 1:1, the conversion of IPA was ∼8 times higher than that in the pure IPA case (Figure 5), giving an increase of ∼4 times in turnover

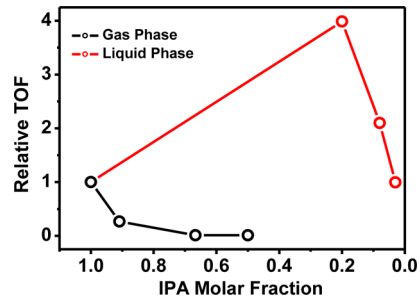


**Figure 5.** Comparison of dependence of catalytic activity on water incorporation in the gas-phase and liquid-phase IPA oxidation reactions catalyzed by 4 nm Pt nanoparticles.

rate. As the oxygen solubility in water is about 10 times lower than that in IPA under the reaction conditions,[14,15] it is clear that water is promoting IPA oxidation catalyzed by Pt nanoparticles. A similar effect of promotion of IPA oxidation by water has been found in our previous study, in which coadsorption of water and IPA on the Pt surface well correlated with enhanced catalytic reaction rates, as evidenced by SFG vibrational spectroscopy.[22] Further lowering of the IPA/water ratio in the mixture led to a decease in TOF (Figure 5), likely due to dilution of the reactant IPA.

To understand more about the water effect in the liquid phase, we investigated the temperature dependence of the reactions catalyzed by Pt nanoparticles with different sizes (Figure S4). In contrast to the size-insensitive activation energy in pure IPA, the activation energy of reaction in the IPA/water mixture was highly impacted by the size of the Pt nanoparticles (Figure S3). The activation energy for 2 nm Pt nanoparticles was ∼13 kJ/mol, which increased to ∼62 kJ/mol for 4 nm ones. With a further increase of particle size, the increasing trend of activation energy started to slow down. The 6 and 8 nm nanoparticles showed activation energies of ∼88 and 91 kJ/mol, respectively. Such differences in activation energy clearly indicate that water alters the reaction mechanism of IPA oxidation in the liquid phase, although at this stage we are not clear about the mechanistic reasons for the observed strong size-dependent activation energy in the IPA/water mixture.

We further studied the effect of water on the IPA oxidation reaction in the gas phase using 4 nm Pt nanoparticles as the catalyst. In stark contrast to the liquid-phase reaction where the


dx.doi.org/10.1021/ja505641r | J. Am. Chem. Soc. 2014, 136, 10515−10520

oxidation rate was drastically increased by the addition of water into IPA, the gas-phase IPA oxidation reaction was strongly inhibited by water vapor. When 1 Torr of water vapor was introduced into the reaction system to give a water/IPA molar ratio of 1:10, the IPA oxidation TOF decreased by 73% (Figure 5). The reaction rate was lowered by ∼100 times when the water vapor was increased to 5 Torr to give a water/IPA molar ratio of 1:2 (Figure 5). The very different roles played by water in the liquid phase compared to the gas phase suggested different reaction pathways for IPA oxidation at the solid/liquid interface compared to the solid/gas interface. It is possible that in the liquid phase water could stabilize the intermediates and/or participate in the catalytic process to promote the reaction, while in the gas-phase reaction water vapor might compete for the active sites and therefore lower the reaction rate.

## DISCUSSION

As shown above, the liquid-phase reaction differs from the gas-phase reaction in the reaction rate, activation energy, dependence of activation energy on nanoparticle size, and effect of water addition. The surprisingly different kinetic results indicate that the reaction mechanisms at the solid/liquid interface vs the solid/gas interface are different as well. To gain a molecular level understanding of such differences, we used SFG vibrational spectroscopy to probe the adsorbed molecules on Pt nanoparticles under IPA oxidation reaction conditions in both the gas phase and the liquid phase. With intrinsic interface sensitivity, SFG vibrational spectroscopy is ideal for examining the molecular adsorbates on the catalyst surface. Under the gas-phase reaction condition, we observed three vibrational features on the surface of 4 nm Pt nanoparticles, corresponding to the symmetric stretch (∼2875 $cm^{-1}$), Fermi resonance mode (∼2940 $cm^{-1}$), and asymmetric stretch (∼2970 $cm^{-1}$) of the methyl groups in IPA species (Figure 6a). In the liquid phase, the increased intensity for the asymmetric stretch and decreased intensity for the symmetric stretch of methyl groups were detected on the 4 nm Pt nanoparticle surface (Figure 6b), indicating different orientations of IPA species at the solid/liquid interface than the solid/gas interface.[23] Fitting these spectra allowed for the amplitude, widths, and centers of the vibrational peaks to be determined (Table S1 and 2).

SFG theory predicts that the intensity ratio of two modes of the same functional group depends primarily on the orientation of that functional group relative to the surface.[23] Kataoka et al. have calculated the orientation dependence of the intensities of methyl stretch modes for IPA using a united atom approach.[24] The united atom method utilizes symmetry arguments to describe the collective contributions of the IPA methyl groups to the SFG signal by a nonlinear susceptibility of the entire isopropyl group with $C_{2v}$ symmetry. Their work includes explicit derivations of the susceptibility elements in lab coordinates as a function of the Euler angles describing the orientation of the isopropyl group. We used their method to calculate the orientation of the IPA molecule in our studies from the ratio of intensities of the $CH_3$ asymmetric and symmetric stretching peaks (see SI for details).

The orientation of the isopropyl group can be fully described by the three Euler angles: $\theta$, $\phi$, and $\chi$, which are the tilt angle of the vector bisecting the C−C bonds in the isopropyl group, the rotational angle of the C−C−C plane with respect to a plane perpendicular to the surface, and the rotation of the bisector around the surface normal. We assumed $C_{\infty v}$ symmetry for the Pt surface and therefore total isotropy for the IPA molecule in the $\chi$ direction (rotation of the molecule around the surface normal). Thus, the molecule could be described by just $\theta$ and $\phi$. With only the ppp polarization combination it is not possible to determine the values of these parameters absolutely, but the value of $\theta$ can be calculated for an assumed value of $\phi$, for instance. Figure S6 shows the intensity ratio as calculated by the united atom method as a function of $\theta$ for a number of assumed values of $\phi$, which are shown in the legend. Here, a low value of $\theta$ describes a molecule with its isopropyl group pointing up from the surface ("standing up") and a high value represents a molecule close to the surface ("lying down"). A high value of $\phi$ describes an isopropyl group with its two methyl groups equidistant to the surface ("surface parallel"), and a low value describes the group rotated perpendicular to the surface ("surface perpendicular"). The bold lines in Figure S6 are the values of the intensity ratios from our experimental data, 0.24 for the gas-phase condition, and 38 for the liquid-phase condition. Possible orientations which would reproduce our spectral intensity ratios to within 20% are plotted in blue in Figure 7a, b. It can be seen that, in the liquid phase, the isopropyl group is relatively surface perpendicular and standing up. But in the gas phase the orientation of the molecule is not as defined. A variety of orientations are possible based on our SFG data.

We employed a computational simulation to further rationalize the orientations of IPA molecules adsorbed on the Pt surface in the gas and liquid phases. Since nanoparticles and nanoparticle−molecule complexes are too large for direct *ab initio* calculations, we simplified our consideration to IPA adsorption on the Pt(111) surface, which is the most stable and

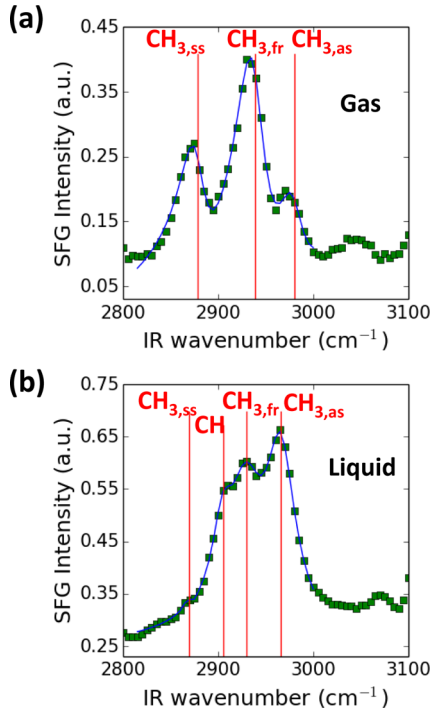


**Figure 6.** SFG vibrational spectroscopy under reaction conditions. (a) SFG vibrational spectrum obtained on the surface of 4 nm Pt nanoparticles under gas-phase reaction conditions. (b) SFG vibrational spectrum obtained on the surface of 4 nm Pt nanoparticles under liquid-phase reaction conditions. The red lines mark the wavenumbers of symmetric stretch ($CH_{3,ss}$ ∼2875 $cm^{-1}$), Fermi resonance mode ($CH_{3,fr}$ ∼2940 $cm^{-1}$), and asymmetric stretch ($CH_{3,as}$ ∼2970 $cm^{-1}$) of the methyl groups and stretch of the CH groups (CH ∼2905 $cm^{-1}$).


dx.doi.org/10.1021/ja505641r | J. Am. Chem. Soc. 2014, 136, 10515−10520

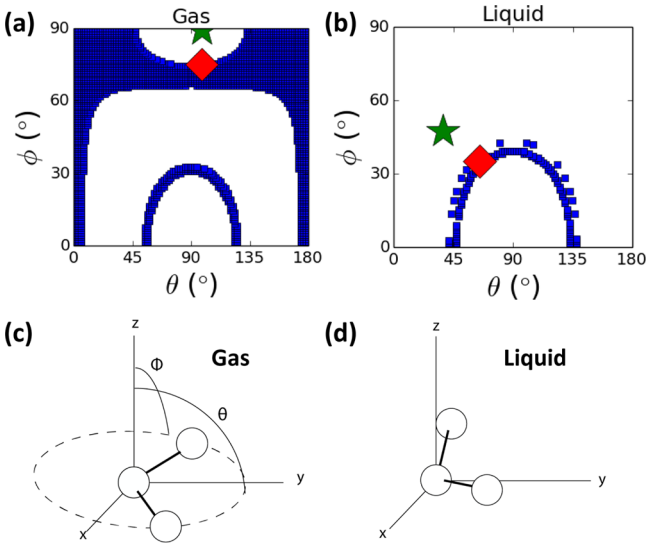


**Figure 7.** Analysis of IPA orientations at solid/liquid and solid/gas interfaces. (a, b) Possible orientations (blue points) of the isopropyl group of IPA in gas phase and liquid phase, which would produce methyl asymmetric/symmetric intensity ratios within 20% of the values in the SFG spectra. The green stars mark the molecular orientations predicted by computational simulation. The red diamonds mark the blue points closest to the green stars. (c, d) Cartoons showing the orientations of the isopropyl group of IPA in the gas phase and liquid phase. Cartoons are plotted to depict orientations noted by the red diamonds in (a) and (b).

dominant facet in Pt catalyst nanoparticles.[25] The constructed systems correspond to two different concentrations of IPA molecules on the Pt surface. The next-nearest distance between atoms of different molecules is more than 7 Å for the small concentration of 0.938 molecules per $nm^2$. At this separation distance, the molecules are considered to have extremely little interaction at the DFT level of theory. Therefore, we assume that the corresponding molecular configuration represents the configuration of IPA molecules adsorbed on Pt nanoparticles from the gas phase. We modeled the large surface concentration with 3.75 molecules per $nm^2$. The value is very close to 3.94 molecules per $nm^2$ as derived from the concentration of $7.85 \times 10^{24}$ molecules per liter for IPA molecules in the liquid phase. The optimized minimum energy configurations for the gas-phase and liquid-phase models are shown in Figure S7. In the gas-phase configuration, the IPA molecules are "lying flat" on the surface with both C−C bonds forming 86° relative to the surface normal, similar to that previously reported.[26] In the liquid phase, the IPA molecules are "standing" on the surface with 38° and 84° orientations of C−C bonds. The change of molecule configuration from "lying flat" to "standing" with the increase of the surface concentration of molecules can be explained by steric molecular interaction: in order to pack more molecules on the surface, molecules are forced to take the "standing" position. Consequently, the effective molecule−surface distance increases leading to a decrease of the molecule−surface interaction and thus a decrease of the adsorption energy (Table S3). We note that the distance between the $\alpha$-C−H and its nearest Pt atom is much larger in the gas-phase condition than in the liquid-phase condition (Table S3). This could explain the much higher activation energy observed for the gas-phase reaction than the liquid-phase reaction, as cleavage of the $\alpha$-C−H bond by Pt is believed to be the rate-determining step in IPA oxidation reactions.[21]

Guided by the theoretical calculation results, we were able to narrow down the orientation possibilities of IPA molecules as suggested by our SFG data. Molecular orientations predicted by computational simulation are marked with green stars in Figure 7a, b for the gas-phase and liquid-phase conditions, respectively. Accordingly, the most likely orientations that match our SFG spectroscopy data are marked with red diamonds in Figure 7a, b, and the corresponding orientations of the isopropyl groups are shown in Figure 7c, d. In the gas phase, the isopropyl group is "lying down" on the Pt surface with both $\theta$ and $\phi$ close to 90°. In the liquid phase, the isopropyl group is both tilted and rotated, giving a "standing up" configuration. Such differences in molecular orientation of IPA adsorbed on the Pt surface may be responsible for the observed distinctive kinetics of the liquid-phase and gas-phase reactions.

## CONCLUSION

In summary, we have studied the IPA oxidation reactions catalyzed by Pt nanoparticles with tunable sizes in both the liquid phase and the gas phase. The liquid-phase reaction differs from the gas-phase reaction in reaction rates, activation energy, dependence of activation energy on nanoparticle size, and effect of water addition. The results indicate different kinetic processes at the solid/liquid interface vs the solid/gas interface for the same reaction. Such differences could be partially due to the different orientations of IPA species on the Pt nanoparticle surface. Further studies will include kinetic measurements of the catalytic oxidation of alcohols with different chemical structures than IPA in gas and liquid phases, as well as SFG spectroscopy in the C−O stretch range to verify the conformations of molecular adsorbates on the catalyst surface.

## ASSOCIATED CONTENT

### Supporting Information

Detailed experimental procedures and supplementary figures and tables are included. This material is available free of charge via the Internet at http://pubs.acs.org.

## AUTHOR INFORMATION

### Corresponding Author

somorjai@berkeley.edu

### Author Contributions

[§]H.W., A.S., and C.M.T. contributed equally.

### Notes

The authors declare no competing financial interest.

## ACKNOWLEDGMENTS

This work was supported by the Director, Office of Basic Energy Sciences,Materials Science and Engineering Division of the U.S. Department of Energy under Contract No. DE-AC02-05CH11231. H.W. acknowledges support from the Philomathia Postdoctoral Fellowship.

## REFERENCES

(1) Liu, H.; Song, C.; Zhang, L.; Zhang, J.; Wang, H.; Wilkinson, D. P. *J. Power Sources* **2006**, *155*, 95.
(2) Zhao, X.; Yin, M.; Ma, L.; Liang, L.; Liu, C.; Liao, J.; Lu, T.; Xing, W. *Energy Environ. Sci.* **2011**, *4*, 2736.
(3) Besson, M.; Gallezot, P. *Catal. Today* **2000**, *57*, 127.
(4) Mallat, T.; Baiker, A. *Chem. Rev.* **2004**, *104*, 3037.

(5) Yu, W. T.; Porosoff, M. D.; Chen, J. G. G. *Chem. Rev.* **2012**, *112*, 5780.
(6) Kim, K. H.; Ihm, S. K. *Journal of Hazardous Materials* **2011**, *186*, 16.
(7) Rylander, P. *Catalytic hydrogenation over platinum metals*; Elsevier: 2012.
(8) Grass, M. E.; Rioux, R. M.; Somorjai, G. A. *Catalysis Letters* **2009**, *128*, 1.
(9) Rioux, R.; Hsu, B.; Grass, M.; Song, H.; Somorjai, G. A. *Catalysis Letters* **2008**, *126*, 10.
(10) Kuhn, J. N.; Huang, W.; Tsung, C.-K.; Zhang, Y.; Somorjai, G. A. *J. Am. Chem. Soc.* **2008**, *130*, 14026.
(11) Pushkarev, V. V.; Musselwhite, N.; An, K. J.; Alayoglu, S.; Somorjai, G. A. *Nano Lett.* **2012**, *12*, 5196.
(12) Wang, H.; Wang, Y.; Zhu, Z.; Sapi, A.; An, K.; Kennedy, G.; Michalak, W. D.; Somorjai, G. A. *Nano Lett.* **2013**, *13*, 2976.
(13) An, K.; Somorjai, G. A. *ChemCatChem.* **2012**, *4*, 1512.
(14) Battino, R.; Rettich, T. R.; Tominaga, T. *J. Phys. Chem. Ref. Data* **1983**, *12*, 163.
(15) Quaranta, M.; Murkovic, M.; Klimant, I. *Analyst* **2013**, *138*, 6243.
(16) Joo, S. H.; Kwon, K.; You, D. J.; Pak, C.; Chang, H.; Kim, J. M. *Electrochim. Acta* **2009**, *54*, 5746.
(17) Shao, M. H.; Peles, A.; Shoemaker, K. *Nano Lett.* **2011**, *11*, 3714.
(18) Mayrhofer, K. J. J.; Blizanac, B. B.; Arenz, M.; Stamenkovic, V. R.; Ross, P. N.; Markovic, N. M. *J. Phys. Chem. B* **2005**, *109*, 14433.
(19) Tritsaris, G.; Greeley, J.; Rossmeisl, J.; Nørskov, J. K. *Catalysis Letters* **2011**, *141*, 909.
(20) Nicoletti, J. W.; Whitesides, G. M. *J. Phys. Chem.* **1989**, *93*, 759.
(21) Dicosimo, R.; Whitesides, G. M. *J. Phys. Chem.* **1989**, *93*, 768.
(22) Thompson, C. M.; Carl, L. M.; Somorjai, G. A. *J. Phys. Chem. C* **2013**, *117*, 26077.
(23) Lambert, A. G.; Davies, P. B.; Neivandt, D. J. *Appl. Spectrosc. Rev.* **2005**, *40*, 103.
(24) Kataoka, S.; Cremer, P. S. *J. Am. Chem. Soc.* **2006**, *128*, 5516.
(25) Holby, E. F.; Greeley, J.; Morgan, D. *J. Phys. Chem. C* **2012**, *116*, 9942.
(26) Salciccioli, M.; Chen, Y.; Vlachos, D. G. *J. Phys. Chem. C* **2010**, *114*, 20155.